Photochemistry and Photobiology, 2006, 82: 1517–1529

Invited Review

New Insights into Lung Surfactant Monolayers Using Vibrational Sum Frequency Generation Spectroscopy

Gang Ma and Heather C. Allen*

Department of Chemistry, The Ohio State University, 100 West 18th Avenue, Columbus, OH

Received 30 June 2006; accepted 23 August 2006; published online 24 August 2006 DOI: 10.1562/2006-06-30-IR-958

ABSTRACT

At the air–water interface, interfacial molecular structure, intermolecular interactions, film relaxation and film respreading of model lung surfactant monolayers were studied using vibrational sum frequency generation (VSFG) spectroscopy combined with a Langmuir film balance. Chain-perdeuterated dipalmitoylphosphatidylcholine (DPPC-*d62*), palmitoyloleoylphosphatidylglycerol (POPG), palmitic acid (PA) and tripalmitin were investigated. In the DPPC-*d62*–PA binary monolayer, PA showed a condensing effect on the DPPC chains. On the contrary, in the DPPC-*d62*–POPG binary monolayer, POPG showed a fluidizing effect on the DPPC chains. In the ternary monolayer system of DPPC-*d62*–POPG–PA, the balance between the fluidizing and the condensing effect was also observed. In addition, the film relaxation behavior of DPPC-*d62* and the enhanced film stability of DPPC-*d62* caused by the addition of tripalmitin were observed. Real-time VSFG was also employed to study the respreading properties of a complex lung surfactant mixture containing DPPC-*d62*, POPG, PA and KL_4 (a mimic of SP-B) peptide, which revealed DPPC enrichment after film compression.

INTRODUCTION

In the work presented here, lung surfactant properties were investigated using model lung surfactant systems. These monolayer systems were probed by using a surface selective nonlinear optical approach, vibrational sum frequency generation (VSFG) spectroscopy, coupled to a Langmuir film balance that simultaneously measures surface tension. The vibrational studies presented provide a better understanding of lung surfactant structure and insight into the functional aspects of lung surfactant.

Lung surfactant forms a monolayer at the air–alveolar hypophase interface and is an essential material for lung function (1–3). This complex mixture of lipids and proteins is secreted by the alveolar type II cells into the hypophase in the form of lamellar bodies, which is then transformed into a unique surfactant assembly, tubular myelin (TM). With the aid of TM, lung surfactant can adsorb rapidly onto the air–alveolar hypophase interface during inhalation, forming a surfactant monolayer covering the alveolar hypophase. A major function of the lung surfactant monolayer is to lower the surface tension inside the alveoli to near-zero values during exhalation. This property eases the work associated with breathing and prevents the collapse of the lung at the end of exhalation.

Endogenous lung surfactant composition varies among different mammalian species to some extent. Generally, lung surfactant contains about 90 wt% lipids and 10 wt% surfactant proteins (4,5). Phospholipids, including phosphatidylcholine, phosphatidylglycerol, phosphatidylethanolamine, phosphatidylinositol and phosphatidylserine, make up the majority of the lipid composition, with dipalmitoylphosphatidylcholine (DPPC) being the major phospholipid component. Other minor lipid components include cholesterol and fatty acids. There are also four types of surfactant proteins, SP-A, SP-B, SP-C and SP-D. SP-A and SP-D are hydrophilic; SP-B and SP-C are hydrophobic and SP-B is considered to be the most important surfactant protein. Functional lung surfactant possesses three essential properties: it must be able to adsorb quickly from the hypophase to the air–water interface; it must be able to reach a near-zero surface tension value at the end of exhalation; and it must be able to respread at the air–water interface quickly during inhalation. Because no single lung surfactant component can have all of the three optimized properties, lung surfactant must be a multicomponent mixture (3).

Deficiency and dysfunction of lung surfactant leads to lung disorders (3). Deficiency of lung surfactant in premature infants results in respiratory distress syndrome (RDS), which is one of the leading causes of infant death (3). Current clinical treatment for RDS is through surfactant replacement therapy, namely, administration of exogenous surfactants. Dysfunction of lung surfactant is a condition associated with acute RDS (ARDS). ARDS is a result of lung injury and can affect patients of all ages. Surfactant replacement therapy for ARDS is less successful as compared with RDS because of the complex pathology of ARDS (6).

A fundamental understanding of lung surfactant structure and function can lead to improvements of the established treatments as well as the invention of novel therapies. To this end, a great deal of fundamental research on lung surfactant structure has been performed in the past several decades. In particular, numerous studies on a variety of model systems have been performed with a variety of surface approaches including Langmuir film balance (7–14),

*Corresponding author email: allen@chemistry.ohio-state.edu (Heather C. Allen)

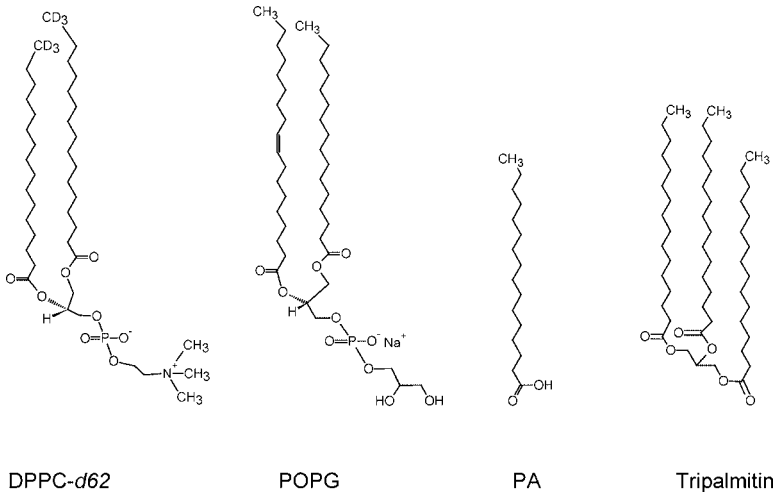

Figure 1. The molecular structures of DPPC-*d62*, POPG, PA and tripalmitin.

pulsating bubble surfactometer (15), captive bubble apparatus (16–20), fluorescence microscopy (FM) (10,21–36), Brewster angle microscopy (BAM) (23,30,31,33–37), atomic force microscopy (27–29,36–39), grazing incidence X-ray diffraction (GIXD) (30,36,40,41), infrared reflection–absorption spectroscopy (42–49), time-of-flight secondary ion mass spectrometry (50–52), attenuated total reflectance FTIR (ATR-FTIR) (53,54) and computer simulation (55–57). Using these physiochemical approaches, scientists have investigated the molecular-level mechanisms, models and concepts to explain the unique lung surfactant properties. For example, three different models, a ''selective adsorption'' model, a ''selective squeeze-out'' model and a ''supercompressed fluid'' model have been proposed to explain how the near-zero surface tension at the end of exhalation is attained (1,2,58,59). A surface-associated reservoir concept has been proposed to explain how surfactant proteins SP-B and SP-C enhance adsorption and respreading of lung surfactant during the breathing cycle (16,26,28,29,32,36,38,49). Details about these breakthroughs can be found in the studies mentioned above and will not be extensively addressed. However, certain details will be addressed as they pertain to the results presented here.

Langmuir monolayers containing either pure or mixtures of lung surfactant components have been widely used as model systems in the *in vitro* research of lung surfactant (3,60). The monomolecular insoluble monolayer at the air–water interface is an excellent model system to mimic *in vitro* some of the lung surfactant properties, such as the surface tension lowering ability during exhalation and the respreading ability during inhalation. Surface pressure, surface density, subphase pH and subphase ionic strength can be easily controlled in this model system.

This paper introduces and summarizes our recent investigations on film condensation, film fluidization, film relaxation and film respreading of selected model lung surfactant Langmuir monolayers using VSFG spectroscopy combined with a Langmuir film balance. In particular, VSFG is employed to gain direct spectroscopic evidence for the underlying intermolecular interactions in these model monolayers. Four lipid components are chosen in our study to construct model lung surfactant monolayers, including chain-perdeuterated DPPC (DPPC-*d62*), palmitoyloleoylphosphatidylglycerol (POPG), palmitic acid (PA) and tripalmitin. These four lipids are key lipid components in endogenous or exogenous lung surfactants (3,61). Using DPPC-*d62* in place of nondeuterated DPPC avoids spectral overlap between DPPC and other lipids. DPPC is the major lipid component in both natural and synthetic lung surfactant; furthermore, all replacement surfactants include DPPC as a major component. POPG represents the phosphatidylglycerol component found in natural lung surfactant. Both PA and tripalmitin are important additives of Survanta, a widely used replacement surfactant in U.S. hospitals. Moreover, DPPC, POPG and PA are the only three lipid components in the all-synthetic replacement surfactant, Surfaxin, a new-generation replacement surfactant (62). In the study presented here, DPPC, POPG, PA and tripalmitin were used to form either neat or mixed monolayers in a Langmuir trough. The pure and mixed monolayers investigated in this work include DPPC-*d62*, DPPC-*d62*–PA, DPPC-*d62*–POPG, DPPC-*d62*–POPG–PA, DPPC-*d62*–tripalmitin and a more complex system containing DPPC-*d62*, POPG, PA and KL_4. KL_4 is an SP-B mimic peptide with 21 amino-acid residues (63).

MATERIALS AND METHODS

Materials. Acyl chain deuterated 1,2-dipalmitoyl-sn-glycero-3-phosphocholine (DPPC-*d62*) and 1-palmitoyl-2-oleoyl-sn-glycero-3-phosphatidylglycerol (POPG) were purchased from Avanti Polar Lipids (Alabaster, AL) with >99% purity. PA and tripalmitin with 99% purities were purchased from Sigma-Aldrich. The KL_4 peptide with an amino acid sequence of KLLLLKLLLLKLLLKLLLLK (K: Lysine; L: Leucine) was custom-synthesized by Biopeptide Co., LLC (San Diego, CA) with a purity of 98% by HPLC. The molecular structures of DPPC-*d62*, POPG, PA and tripalmitin are shown in Fig. 1. Spectrophotometric grade chloroform and methanol were purchased from Sigma-Aldrich. Deionized water was from a Barnstead Nanopure system with a resistivity of 18.2 MΩ • cm. Ethylenediaminetetraacetic acid (EDTA) disodium salt, hydrochloric acid, Trizma (tris(hydroxymethyl) aminomethane base) and sodium chloride were obtained from Fisher Scientific.

Sample preparation. Stock solutions of DPPC-*d62*, PA and tripalmitin with concentrations of 1 m*M* were made in chloroform; stock solution of POPG with a concentration of 1 m*M* was made in chloroform/methanol (3/1 vol/vol); stock solution of KL_4 with a concentration of 0.65 mg/mL was made in chloroform/methanol (3/1 vol/vol). These solutions were mixed in appropriate ratios to form model lung surfactant mixtures. The subphase used in the monolayer measurements was pure water with a measured pH value of 5.5. However, an aqueous solution consisting of 100 m*M* NaCl and 0.1 m*M* EDTA in 5 m*M* tris buffer at pH of 7 was used as the subphase for the respreading experiment.

Methods. As shown in Fig. 2, the VSFG investigation is performed on the monolayer spread in a Langmuir film balance. Details about the Langmuir film balance experiments and the VSFG experiments are provided as follows.

Langmuir film balance. The monolayer compression and expansion were performed in a Langmuir trough (KSV minitrough, KSV, Finland). The rectangular trough (176.5 × 85 mm) is made of Teflon and was

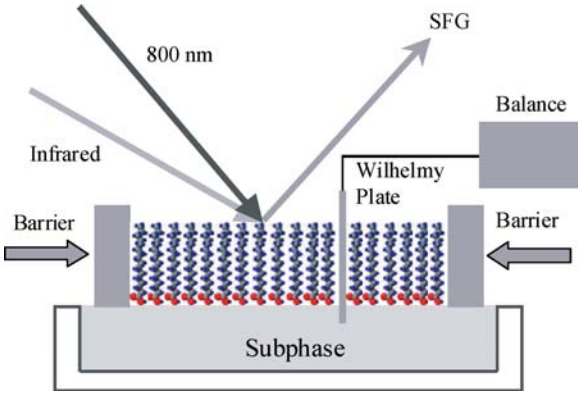

Figure 2. BBSFG experiment coupled to a Langmuir film balance.

thermostated by circulating water in channels placed underneath the trough at a temperature of 24 ± 0.5°C. Two barriers are employed to provide symmetric film compression. The barriers were made of Delrin, a hydrophilic material, which prevents leakage of the monolayer beneath the barriers. The surface pressure and the mean molecular area (or trough area) were continuously monitored during film compression and expansion by the Wilhelmy plate method. The plate is made of platinum or filter paper (paper plate was used in the respreading experiment). The platinum plate was flamed with a Bunsen burner before each run of experiment. The trough was filled with pure water (or the buffer solution). Before spreading surfactant, the subphase surface was swept by the barriers to ensure that no significant surface pressure increase occurred. A known amount of the lung surfactant solution was spread on the subphase in a drop-wise manner with a Hamilton syringe, and 10 min was allowed to elapse for complete solvent evaporation before starting the compression. The same barrier moving speeds (5 mm/min) were used for film compression and expansion.

Broad-bandwidth VSFG. There are two types of VSFG technologies, scanning VSFG and broad-bandwidth SFG (BBSFG). In this study, the BBSFG system was employed. The BBSFG laser system in our lab consists of two 1-kHz repetition rate regenerative amplifiers (Spitfire, fs and ps versions, Spectra-Physics), both of which are seeded by sub-50 fs 792 nm pulses (the wavelength is tuned for system optimization) from a Ti: Sapphire oscillator (Tsunami, Spectra-Physics) and pumped by a 527 nm beam from an all solid-state Nd:YLF laser (Evolution 30, Spectra-Physics). The two regenerative amplifiers provide 85 fs pulses at 800 nm (22 nm bandwidth) and 2 ps pulses at 800 nm (17 cm^{-1} bandwidth). The fs broad-bandwidth pulses were then used to generate broad-bandwidth infrared light via an optical parametric amplifier (OPA-800CF, Spectra-Physics). The wavelength tuning ability of the OPA is achieved by adjusting the phase-matching angles of the BBO and $AgGaS_2$ crystals. The spectral window of the broad IR pulse can be as large as 500 cm^{-1} depending on the tuned spectral region. Therefore, using a BBSFG system, a surface vibrational spectrum can be obtained without wavelength scanning. In this work, the output energy of each 800 nm ps pulse was 300 μJ for most of the experiments and 400 μJ for the respreading investigation. The IR energy was 6 μJ per pulse in the C-D stretching region; 9 μJ per pulse in the C-H stretching region; and 1 μJ per pulse in the PO_2^--SS stretching region. As shown in Fig. 2, the Langmuir film balance was placed on the sample stage of the BBSFG system. The 800 nm ps beam and the spectrally broad IR beam were overlapped at the monolayer surface spatially and temporally. The generated SFG signal containing spectral information from the monolayer was detected using a monochromator–CCD detection system (SpectraPro SP-500 monochromator with a 1200 g/mm grating blazed at 750 nm, Acton Research; 1340 × 400 pixel array, LN400EB back-illuminated CCD, Roper Scientific). Typical spectral acquisition time was 5 min.

The SFG spectrum is polarization dependent. In this study, the polarization combination of ssp (s–SFG; s–800 nm; p–infrared) was used. The SFG spectrum was normalized against a nonresonant SFG spectrum from a GaAs crystal (Lambda Precision Optics, Inc.) to remove the spectral distortion caused by the energy profile of the infrared pulse. To calibrate the SFG peak positions, a nonresonant SFG spectrum from the GaAs crystal surface was obtained with a polystyrene film covering the OPA infrared output port. The resulting SFG spectrum containing polystyrene infrared absorption bands was used for the calibration. The calibration accuracy is better than 1 cm^{-1}.

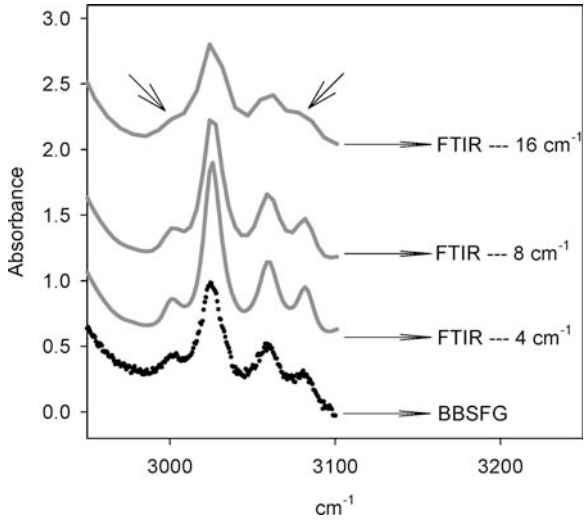

Figure 3. Infrared absorption spectra of a polystyrene film taken with BBSFG laser system and FTIR spectrometer with different spectral resolutions.

The spectral resolution of the BBSFG system was characterized with an approach proposed by Ishibashi and Onishi (64). A polystyrene IR transmission spectrum was obtained with the BBSFG system using a polystyrene film to cover the output port of the OPA. The IR transmittance was then converted into absorbance. The absorption spectrum obtained with BBSFG was compared with the absorption spectra taken with a commercial FTIR spectrometer (Avatar 370, Thermo Nicolet) under three different spectral resolutions, 4, 8 and 16 cm^{-1}. As shown in Fig. 3, the two arrows indicate the positions of two polystyrene absorption bands. The two bands are not well resolved in the FTIR spectrum with 16 cm^{-1} resolution and appear as shoulders. However, the two bands are well resolved in the FTIR spectra with 4 cm^{-1} and 8 cm^{-1} resolutions as well as in the IR absorption spectrum taken with the BBSFG system. Furthermore, the IR absorption spectrum of polystyrene taken with the BBSFG system is quite similar in spectral resolution to that of the FTIR spectrum with 8 cm^{-1} resolution. (The Thermo Nicolet Avatar 370 limits our accessible IR resolutions to 1, 2, 4, 8 and 16 cm^{-1}.) Therefore, the spectral resolution of the BBSFG system is closest to the 8 cm^{-1} infrared resolution.

The BBSFG system combined with the Langmuir film balance can work in three different modes: pause mode, hold mode and real-time mode. In pause mode, the barriers compress the monolayer to a given surface pressure and halt; a BBSFG spectrum is then taken during the halting period. During the pausing period, the film usually experiences a surface pressure drop (also called film relaxation) (3). Because the BBSFG system requires relatively short spectral acquisition times, the pressure drop was found to have a negligible effect on the obtained BBSFG spectrum. In hold mode, the barriers move to hold the surface pressure at a given value and a BBSFG spectrum is then taken during the holding period. With the real-time mode, the BBSFG spectra were taken simultaneously during film compression and expansion. In our studies, the pause mode and the hold mode gave identical spectra. The real-time mode was utilized to investigate the film relaxation and film respreading. Other investigations were completed under either pause mode or hold mode.

VSFG background. Since its inception in 1987 (65–67), VSFG has become a powerful surface-probing technique in a variety of research fields, including materials science, atmospheric chemistry, environmental science and bioscience (68–84). SFG utilizes two pulsed laser beams with different frequencies to probe the surface. The two incident pulses generate a third frequency at the sum of the incident frequencies. Typically, one incident beam is in the visible region and the other is in the infrared region. When the infrared pulse is resonant with a surface vibrational mode of the molecule at the surface, an SFG signal enhancement is observed and the enhanced signal provides a surface vibrational spectrum. VSFG is a unique surface vibrational spectroscopic technique owing to its intrinsic surface selectivity derived from its selection rule requiring lack of inversion symmetry. VSFG also requires the surface vibrational mode to be both infrared-active and Raman-active.

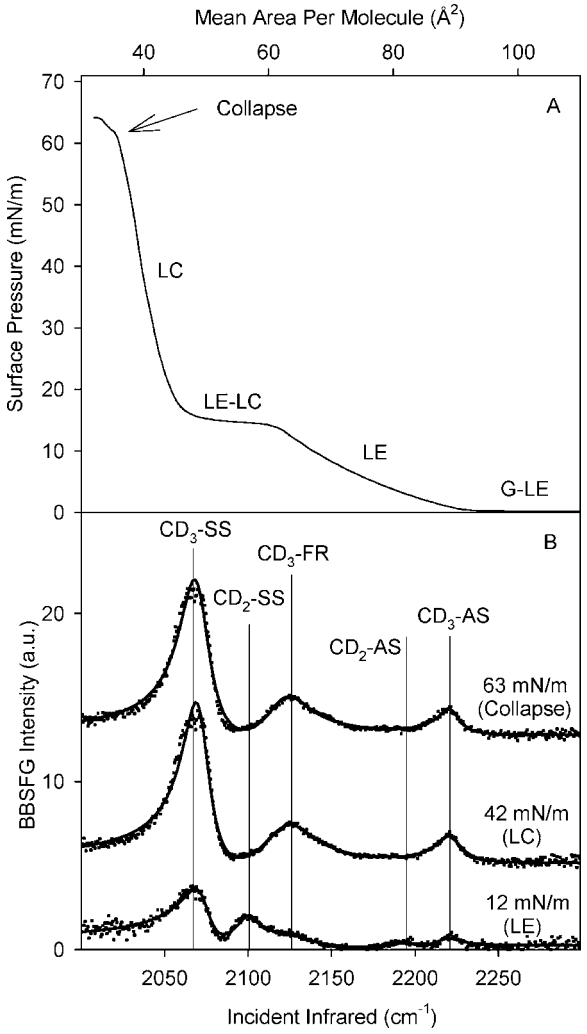

Figure 4. A: Surface pressure–area isotherm of DPPC-*d62* monolayer on a pure water subphase at 24°C. B: BBSFG spectra of DPPC-*d62* in the C-D stretching region with spectral assignments at different surface pressures. G is the gas phase; LE is the liquid-expanded phase; LC is the liquid-condensed phase; solid lines in B are spectral fits.

The SFG intensity, I_{SFG}, as shown in Equation (1),

$$I_{SFG} \propto |\chi^{(2)}|^2 \propto \left|\chi^{(2)}_{NR} + \sum_v \chi^{(2)}_v\right|^2 \quad (1)$$

is proportional to the absolute square of the macroscopic second order susceptibility, $\chi^{(2)}$, which consists of resonant terms ($\chi^{(2)}_v$) and a nonresonant term ($\chi^{(2)}_{NR}$). When the frequency of an incident infrared beam, ω_{IR}, is resonant with a vibrational mode, v, the resonant susceptibility term ($\chi^{(2)}_v$) dominates the nonlinear susceptibility ($\chi^{(2)}$) and an SFG intensity enhancement is observed. The resonant macroscopic nonlinear susceptibility, $\chi^{(2)}_v$, is shown in equation (2),

$$\chi^{(2)}_v \propto \frac{A_v}{\omega_{IR} - \omega_v + i\Gamma_v} \quad (2)$$

where A_v is the strength of the transition moment, v is the frequency of the transition moment and Γ_v is the linewidth of the transition. The strength, A_v, is nonzero when the Raman and the infrared transitions are both spectroscopically allowed. $\chi^{(2)}_v$ is related to the molecular hyperpolarizability, β_v, shown in equation (3), by the number density of the surface species, N, and an orientationally averaged Euler angle transformation, $\langle\mu_{IJK:lmn}\rangle$, between the laboratory coordinates (I, J, K) and the molecule coordinates (l, m, n) (73,85,86).

$$\chi^{(2)}_v = N\sum_{lmn}\langle\mu_{IJK:lmn}\rangle\beta_v \quad (3)$$

As shown in equations (1), (2) and (3), the SFG spectrum contains information about surface molecular density, molecular moiety interfacial orientation and surface vibrational frequency. These three parameters are extremely valuable in characterizing interfacial structure, molecular interactions and interfacial properties.

RESULTS AND DISCUSSION

DPPC-*d62* Langmuir monolayer

DPPC is the major lipid component in lung surfactant and plays a central role in surface tension lowering during exhalation. Therefore, initial studies (87) were performed solely on a DPPC monolayer on a pure water subphase to understand the surface structural properties in different interfacial phases. In addition, as the model lung surfactant mixtures in our studies increased in complexity, using deuterated DPPC allowed us to probe the mixed monolayer with minimal spectral interference. Therefore, these initial studies were performed on DPPC-*d62*.

Surface pressure–area isotherm measurements are a common way to characterize Langmuir monolayers (88), and thus isotherm measurements were performed before the VSFG investigations as a standard procedure. Figure 4A shows the surface pressure–area isotherm of DPPC-*d62* at 24°C on a pure water subphase. In the isotherm, each slope change of the isotherm indicates a phase transition (88). Figure 4A shows five different phase regions. Following the general assignments in the literature, these phase regions have been assigned to be G-LE, LE, LE-LC, LC and collapse (89). G is the gas phase; LE is the liquid-expanded phase; LC is the liquid-condensed phase (also called the tilted-condensed phase); G-LE is the coexistence of the G and LE phases; LE-LC is the coexistence of the LE and LC phases. Collapse refers to the situation in which the two-dimensional monolayer is broken and a three-dimensional structure forms. DPPC-*d62* has the LE-LC phase transition at the surface pressure of 15 mN/m, which is about 10 mN/m higher than that of the nondeuterated DPPC. As shown in Figure 4A, the DPPC-*d62* monolayer collapses at 63 mN/m. The collapse pressure of DPPC can reach above 70 mN/m if the Langmuir trough is equipped with a ribbon barrier (7).

To gain molecular level insights on DPPC interfacial structure, VSFG spectroscopy was employed to investigate the DPPC-*d62* monolayer as stated above. Numerous BBSFG spectra were obtained under different surface pressures along the isotherm; three representative spectra are shown in Fig. 4B. The three spectra correspond to DPPC-*d62* in three different phases: LE, LC and collapse. These spectra were acquired when the infrared energy was tuned into the C-D stretching region of 2000 to 2300 cm^{-1}, thereby providing structural information of the deuterated hydrocarbon chains of DPPC-*d62*. At 12 mN/m, there are five peaks revealed in the spectrum. These peaks are located at 2073, 2102, 2121, 2194 and 2221 cm^{-1}. As denoted by the vertical lines in Fig. 4B, these five peaks are assigned to the CD_3 symmetric stretching (CD_3-SS), CD_2 symmetric stretching (CD_2-SS), CD_3 Fermi-resonance (CD_3-FR), CD_2 asymmetric stretching (CD_2-AS) and CD_3 asymmetric stretching (CD_3-AS) modes, respectively. The spectral assignments are based on previous vibrational spectroscopic studies on deuterated DPPC (90,91). At 42 mN/m and 63 mN/m, only three peaks, the CD_3-SS, CD_3-FR and CD_3-AS, are observed in the BBSFG spectra. The distinct difference between the 12 mN/m spectrum and the 42 mN/m spectrum lies in

the presence or absence of the CD_2-SS and CD_2-AS peaks in the two spectra. This reflects the molecular conformation difference between the LE phase and the LC phase. In the LE phase, DPPC molecules behave like a two-dimensional liquid. The hydrocarbon chains adopt flexible gauche conformations. There is a lack of inversion symmetry in each pair of methylene groups in gauche configurations. The lack of inversion symmetry makes both the CD_2-SS and CD_2-AS modes SFG active. Therefore, the two peaks show up in the 12 mN/m spectrum. In contrast to the LE phase, the LC phase is similar to a two-dimensional semicrystalline phase. The absence of the CD_2 peaks in the 42 mN/m spectrum indicates that the hydrocarbon chains of DPPC in the LC phase adopt an all-trans configuration. The all-trans configuration generates inversion symmetry in each trans pair of methylene groups. Because DPPC has an even number of methylene groups, no CD_2 stretches can be SFG active. Therefore, both the CD_2-SS and CD_2-AS disappear from the 42 mN/m spectrum.

The 12 and 42 mN/m spectra shown here demonstrate the capability of VSFG spectroscopy to probe the molecular conformation of lipids at the interface during a Langmuir trough compression. We later show the employment of this capability to investigate chain-chain interactions between different types of lipids.

Figure 4B also shows that the 42 mN/m BBSFG spectrum is nearly identical to the BBSFG spectrum of DPPC in the collapse phase. This phenomenon can be explained in the following way. According to the generally accepted collapse mechanism, lipids in collapse phase will form trilayer-structure patches (92,93). The trilayer-structure patch consists of a monolayer plus a bilayer that is either underneath or on top of the monolayer. The presence of inversion symmetry in the bilayer structure makes the bilayer SFG-inactive (80). Consequently, although the surface number density of the collapse region is tripled, the trilayer-structure patch behaves like a monolayer with respect to the power of producing SFG intensity. Therefore, it is not surprising to observe that the SFG spectra remain nearly unchanged before and after collapse.

DPPC-*d62*–PA mixed monolayer

Palmitic acid is an important additive in several exogenous surfactant preparations, such as Survanta and Surfaxin (3). VSFG spectra, as shown in this section, provide molecular level insight by elucidating the interfacial structure and intermolecular interactions between DPPC and PA. FM and GIXD have been used previously to investigate the effect of PA on DPPC monolayers (30,41). FM revealed that adding increasing amounts of PA into the DPPC monolayer increases the area occupied by solid domains. A GIXD study indicated that adding increasing amounts of PA to the condensed phase of DPPC decreased the overall chain tilt angle significantly. These effects have been referred to as a condensing effect. From a molecular view, the condensing effect is an interfacial ordering effect.

Compared with the previously used surface techniques such as FM and GIXD, VSFG has distinct advantages. First, as an intrinsic vibrational spectroscopic technique, VSFG has functional-group sensitivity. This means that VSFG can probe different moieties of a lipid molecule and can reveal more detailed structural information, which is critical to the study of mixed monolayers such as DPPC with PA. For example, with the use of VSFG to probe both the tail groups and the head groups, the chain-chain interaction and head-head interaction between lipids can be investigated separately. Second, unlike GIXD that probes lipids in a condensed phase, VSFG can probe lipids in both the LE phase and the LC phase. The above two distinct characteristics make VSFG able to provide new insights on lipid-lipid intermolecular interactions that are not accessible by microscopic techniques or X-ray diffraction. The following section summarizes a portion of our recent study on a DPPC–PA monolayer using VSFG (94). This work demonstrates the capability of VSFG to provide direct spectroscopic evidence for the condensing effect of PA on DPPC in the LE phase and reveals that the condensing effect is a conformational ordering effect. Moreover, we also present exciting new results about the head group interaction associated with the condensing effect by probing the phosphate functional group of DPPC.

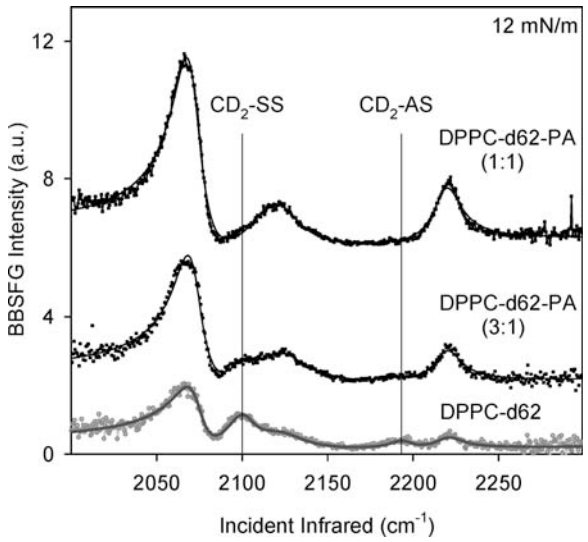

Figure 5. BBSFG spectra of DPPC-*d62* monolayer and DPPC-*d62*–PA mixed monolayers in the C-D stretching region at 12 mN/m on a pure water subphase at 24°C. Solid lines are spectral fits; vertical lines indicate peak positions of the CD_2-SS and the CD_2-AS; (3:1) and (1:1) are the molar ratios between DPPC-*d62* and PA.

The basic approach of using VSFG to investigate intermolecular interactions between PA and DPPC is to analyze the spectral variation of DPPC induced by the addition of PA. The observed spectral variation not only serves as direct evidence for the existence of the intermolecular interaction, but also reveals the molecular nature of the interaction.

Figure 5 shows the BBSFG spectra of DPPC-*d62* in the C-D stretching region in DPPC-*d62*–PA mixed monolayers at the surface pressure of 12 mN/m on a pure water subphase in the C-D stretching region. The 12 mN/m spectrum of DPPC-*d62* in Fig. 4B is shown in Fig. 5 again as the gray curve for reference. As indicated by Fig. 5, the addition of PA has a dramatic effect on the chain conformation of DPPC. The BBSFG spectrum of DPPC-*d62* in the DPPC-*d62*–PA mixture with a 3:1 molar ratio between DPPC-*d62* and PA shows a substantial decrease of the relative intensity ratio of the CD_2-SS to the CD_3-SS ($I_{CD2\text{-}SS/CD3\text{-}SS}$) and the CD_2-AS to the CD_3-AS ($I_{CD2\text{-}AS/CD3\text{-}AS}$) as compared with the reference DPPC-*d62* monolayer (the gray curve). (The spectral parameter of the relative intensity ratio between the methylene group and the methyl group symmetric stretching bands has been used in previous SFG studies to reveal the chain ordering of the hydrocarbon chains; the smaller the ratio, the higher the chain ordering [69–71].) Fitting results further reveal that $I_{CD2\text{-}SS/CD3\text{-}SS}$ dropped from 0.52 for DPPC-*d62* to 0.029 for the DPPC-*d62*–PA (3:1) mixture and $I_{CD2\text{-}AS/CD3\text{-}AS}$ dropped from 0.45 for the DPPC-

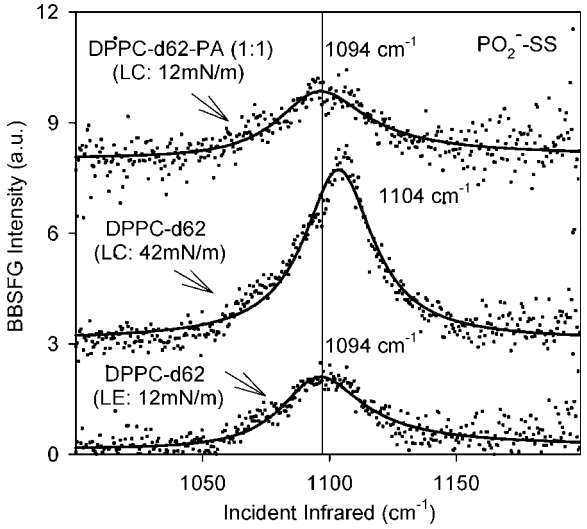

Figure 6. BBSFG spectra of DPPC-*d62* monolayer and DPPC-*d62*–PA mixed monolayers in the PO_2^--SS stretching region on a pure water subphase at 24°C. Solid lines are spectral fits; vertical lines indicate the frequency shift of PO_2^--SS; (1:1) is the molar ratio between DPPC-*d62* and PA.

d62 monolayer to 0.014 for the DPPC-*d62*–PA (3:1) mixture. Results here show that the addition of PA induces the chain ordering of DPPC. When the PA concentration in DPPC-*d62* is further increased, additional changes in the chain ordering results. As is shown in the BBSFG spectrum of the 1:1 mixture in Fig. 5, both the CD_2-SS and the CD_2-AS peak intensities vanish, implying that the DPPC chains adopt an all-trans configuration in the mixed monolayer. The SFG results shown here clearly demonstrate that PA decreases the amount of the gauche defects in the DPPC chains and that the condensing effect is a conformational ordering effect. The observed VSFG results in this study are consistent with VSFG results observed in a cholesterol–DPPC mixed monolayer from recent research performed by Bonn et al. (81).

The physical nature of the chain-chain interaction between DPPC and PA can be described with a mechanism proposed in previous computer simulation investigations on the condensing effect of cholesterol on DPPC chains. A Monte Carlo study on the DPPC–cholesterol mixed monolayer demonstrated that each cholesterol molecule could hinder the rotameric freedom of five to seven DPPC chains (95). A molecular dynamics simulation on the cholesterol effect of DPPC bilayers revealed that the rigid cholesterol ring increased the ordering parameters of its neighboring DPPC chains (96). Analogous to the conceptual interpretation for the condensing effect of cholesterol on DPPC chains, we propose that the resulting conformational ordering of DPPC chains caused by PA is because of the fact that the rotational isomerization of the DPPC chains is hindered by the rigid PA molecules. When there are enough PA molecules present in the mixture, the phase of DPPC will be shifted to a fully condensed phase, as demonstrated in the (1:1) DPPC–PA mixture spectrum in Fig. 5.

The head group interaction between DPPC and PA was also investigated in the fingerprint region with VSFG. Figure 6 shows three BBSFG spectra of the phosphate group symmetric stretch (PO_2^--SS) of DPPC-*d62* in the region of 1000 to 1200 cm^{-1}. The spectral assignment of this peak is from previous infrared and Raman studies of phosphatidylcholines (97–100). The three spectra correspond to the DPPC monolayer at 12 mN/m, the DPPC monolayer at 42 mN/m and the DPPC-*d62*–PA mixed monolayer with a 1:1 molar ratio at 12 mN/m. At 12 mN/m, DPPC-*d62* is in the LE phase. Because of the large mean area occupied by the lipid head in the LE phase, the head group is well solvated by water molecules. Because the hydrogen bonding formation and interaction weakens the PO_2^- bond, the PO_2^--SS is at a lower frequency of 1094 cm^{-1} relative to that in a dehydrated state. Compressing the DPPC-*d62* monolayer into the LC phase causes dehydration of the phosphate group of DPPC-*d62*. The breaking of the hydrogen bonding network of the phosphate group solvation sphere strengthens the PO_2^- bond (101). Consequently, at 42 mN/m, the PO_2^--SS is blueshifted to a higher frequency of 1104 cm^{-1}. As just discussed, the condensing effect of PA shifts the phase of DPPC-*d62* from the expanded phase into a condensed phase, even though the surface pressure is at 12 mN/m. This phase transition, LE to LC, is associated with a dehydration process of the head group of DPPC. Therefore, one might expect the PO_2^--SS frequency of the DPPC-*d62*–PA mixture to be closer to that of the DPPC-*d62* monolayer at 42 mN/m, 1104 cm^{-1}, to correspond to the dehydration. However, the PO_2^--SS frequency of the DPPC-*d62*–PA mixture is 1094 cm^{-1}, clearly redshifted from the 42 mN/m spectrum. This indicates an intermolecular interaction between PA and DPPC. We assert that PA forms a hydrogen bond with the phosphate group of DPPC. The formation of the hydrogen bond between PA and DPPC counteracts the dehydration of the phosphate group associated with the condensing effect. Recall that the pH of water keeps PA from being ionized at the air–water interface (23); therefore, PA has available a COOH hydrogen to form the hydrogen bond with DPPC.

DPPC-*d62*–POPG mixed monolayer

POPG represents the unsaturated and anionic component found in endogenous and exogenous lung surfactants. The role of the unsaturated and anionic components in replacement surfactants is to improve the respreading and adsorption properties of DPPC (3,5). Proper lung surfactant function requires a balance between the saturated rigid components (such as DPPC and PA) and the unsaturated and anionic components (such as POPG) (3). At room and body temperatures, POPG forms fluid films (30). Counter to the condensing effect of PA, POPG has a fluidizing effect on DPPC because of its own fluid nature. The fluidizing effect is essentially an interfacial disordering effect on the molecules within the film. In this section, it is shown that POPG has a conformational disordering influence on the DPPC chains when DPPC is in the LE phase. We also find that when DPPC is in the LC phase, POPG has no effect on the conformational ordering of the DPPC chains.

Figure 7 shows the BBSFG spectrum of DPPC-*d62* in the DPPC-*d62*–POPG mixture at 12 mN/m on a pure water subphase in the C-D stretching region. The gray curve is the 12 mN/m spectrum of DPPC-*d62* shown for reference. The spectral variation caused by the presence of POPG clearly suggests an intermolecular interaction between DPPC and POPG because the DPPC–POPG spectrum is now dominated by the methylene asymmetric stretch. By analyzing the two spectra in Fig. 7, we see two features that support that POPG has a conformational disordering effect on the DPPC chains. The first feature is the variation of $I_{CD2\text{-}AS/CD3\text{-}AS}$, as indicated by the fitted subpeak areas in Fig. 7. Quantitatively, the $I_{CD2\text{-}AS/CD3\text{-}AS}$ values increased from 0.45 for DPPC-*d62* to 59 for the DPPC-*d62*–POPG mixture. The higher the ratio, the more

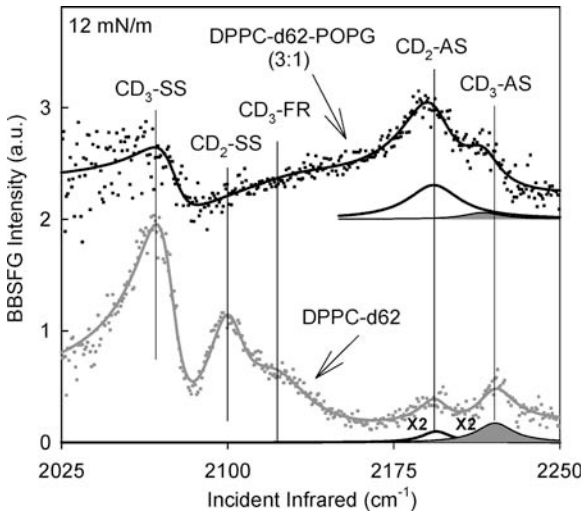

Figure 7. BBSFG spectra of DPPC-*d62* monolayer and DPPC-*d62*–POPG mixed monolayers in the C-D stretching region with spectral assignments at 12 mN/m on a pure water subphase at 24°C. Solid lines are the spectral fits; (3:1) is the molar ratio between DPPC-*d62* and POPG; ×2 is the factor of two magnification of the subpeaks denoted.

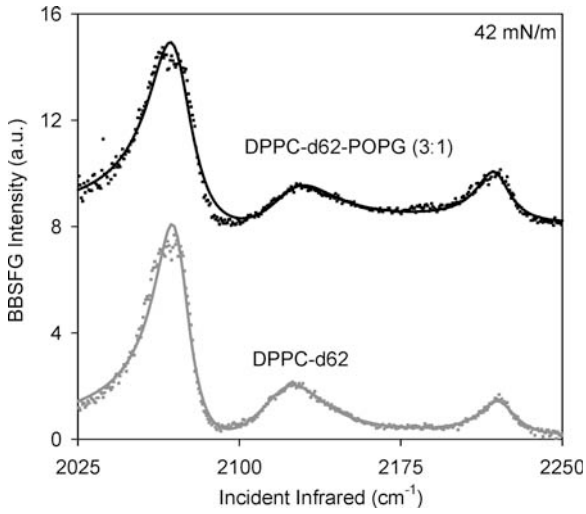

Figure 8. BBSFG spectra of DPPC-*d62* monolayer and DPPC-*d62*–POPG mixed monolayers in the C-D stretching region at 42 mN/m on a pure water subphase at 24°C. Solid lines are spectral fits; (3:1) is the molar ratio between DPPC-*d62* and POPG.

disordered the hydrocarbon chain, as shown above in the study of the DPPC-*d62*–PA monolayer. The second spectral feature is the broadening of the CD_2-AS peak. With the addition of POPG to the DPPC film, the CD_2-AS FWHM bandwidth increased from 16 cm^{-1} for the DPPC-*d62* film to 28 cm^{-1} for the DPPC-*d62*–POPG mixture film. This indicates an increase in gauche defects and thus chain disordering, and is consistent with previous Raman investigations on phospholipids. Raman line broadening has been attributed to the increased gauche defects in hydrocarbon chains (102). For example, dramatic increases in the bandwidths of both the CD_2-SS and the CD_2-AS peaks have been found at the melting temperature of phospholipid films (102). The two spectral features discussed above clearly indicate that POPG further disorders the already disordered DPPC chains in the LE phase. Additionally interesting in the DPPC-*d62*–POPG spectrum of Fig. 7 is that the CD_2-SS band is missing but the CD_2-AS band clearly dominates the spectrum. This may be relevant to the disordered state of the DPPC chains. To elucidate its physical origin requires further investigation.

The DPPC-*d62*–POPG mixed monolayer was also investigated at 42 mN/m. Shown in Fig. 8 are the BBSFG spectra of DPPC-*d62* of the DPPC-*d62* monolayer and the DPPC-*d62*–POPG mixed monolayer. The gray 42 mN/m DPPC-*d62* spectrum from Fig. 4 is shown again in Fig. 8 for reference. The two spectra are nearly identical to each other, with the exception that the DPPC-*d62* monolayer spectrum has a higher absolute intensity in all of the peaks, revealing a lower number density of DPPC-*d62* in the laser probe region for the DPPC-*d62*–POPG mixture. This indicates that there is a phase separation between DPPC-*d62* and POPG. At 42 mN/m, DPPC-*d62* is in the LC phase, forming a highly-packed semicrystalline structure. POPG, because of its cis C=C bond, cannot form a highly-packed crystalline structure. The BBSFG experiment probes both types of domains, yet the incident IR is only resonant with the deuterated domains of the DPPC-*d62*. Clearly, at 42 mN/m, the two lipids are not miscible and a phase separation occurs. Because of the phase separation, POPG does not affect the chain packing of DPPC-*d62* when DPPC is in the LC phase.

DPPC-*d62*–POPG–PA mixed monolayer

In summary of the studies on the DPPC LE phase presented above, Fig. 9 illustrates the condensing effect and the fluidizing effect on the DPPC chain ordering. PA conformationally orders the DPPC chains and POPG conformationally disorders the DPPC chains. This is very different from what was observed from POPG and DPPC when DPPC is in the LC phase region of the isotherm. The balance between these two effects in the LE phase region of the DPPC-*d62*–POPG–PA mixed monolayer was investigated and the results are discussed below.

Figure 10 shows three BBSFG spectra of DPPC-*d62* at 12 mN/m on a pure water subphase in three different mixtures with different lipid molar ratios: DPPC-*d62*–POPG (3:1), DPPC-*d62*–POPG–PA (3:1:1) and DPPC-*d62*–POPG–PA (3:1:3). The spectrum of the 3:1 molar ratio mixture of DPPC-*d62*–POPG is shown here again for comparison. The fitted subpeaks of the CD_2-AS and the CD_3-AS are shown in Fig. 10 to reveal the variation in their intensity ratio, $I_{CD2\text{-}AS/CD3\text{-}AS}$. Adding PA decreases the $I_{CD2\text{-}AS/CD3\text{-}AS}$, indicating an increase in the chain ordering of DPPC-*d62*. As mentioned above, the value of the $I_{CD2\text{-}AS/CD3\text{-}AS}$ for the DPPC-*d62*–POPG mixed film is 59. This ratio decreases to 0.7 in the (3:1:1) DPPC-*d62*–POPG–PA mixture and further decreases to 0.2 in the (3:1:3) DPPC-*d62*–POPG–PA mixture. Figure 10 demonstrates that the fluidizing ability of POPG can be counteracted by the condensing ability of PA. The balance between the fluidizing effect and the condensing effect can be further explained from the viewpoint of the phase behavior variation with the monolayer composition change in the DPPC-POPG–PA system. Previous surface pressure–area isotherms, FM, BAM and GIXD investigations on the DPPC-POPG–PA system demonstrated that adding PA increases the condensed phase fraction in the mixed monolayer, and the condensed phase domains contain DPPC and PA (30). The results shown in Fig. 10 support this scenario. By increasing the condensed phase domain fraction with the addition of PA, the LE phase characteristic peak of the CD_2-AS decreases and the condensed phase characteristic peak of the CD_3-AS increases. Consequently, $I_{CD2\text{-}AS/CD3\text{-}AS}$ decreases as

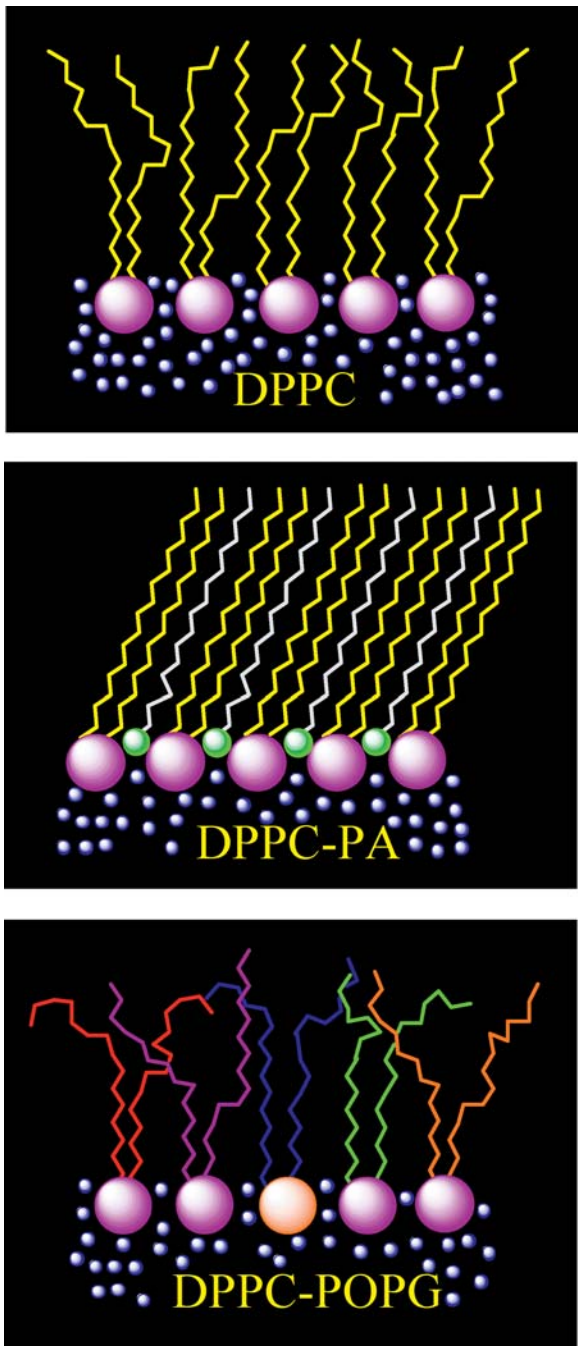

Figure 9. The condensing effect *versus* the fluidizing effect: DPPC illustrated in the LE phase; DPPC ordering because of the addition of PA; and DPPC showing additional disordering because of the addition of POPG.

revealed in Fig. 10. In addition, as shown in Fig. 10, even in the monolayer of DPPC-POPG-PA (3:1:3), the CD_2-AS peak still exists, revealing that DPPC molecules distribute themselves into both the condensed and expanded phases.

It is important to note that these molecular film characteristics, condensation *versus* fluidization capabilities of various lipids, have a profound effect on lung surfactant function, that is, fine-tuning the two effects can alter the balance between the LE and the LC phases under a given surface pressure.

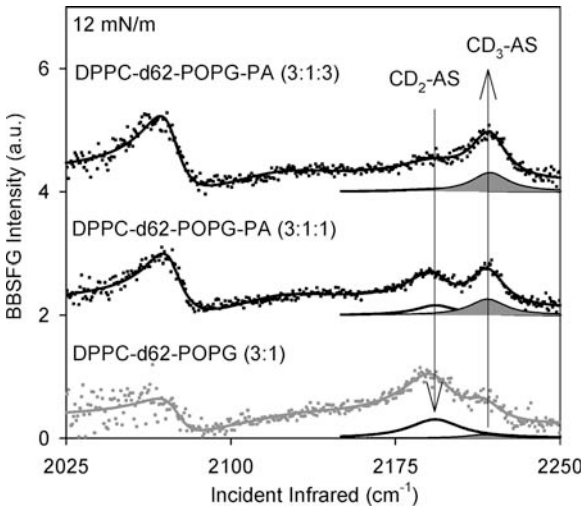

Figure 10. BBSFG spectra of DPPC-*d62*–POPG mixed monolayer and DPPC-*d62*–POPG–PA mixed monolayers in the C-D stretching region at 12 mN/m on a pure water subphase at 24°C. Solid lines are spectral fits; (3:1), (3:1:1) and (3:1:3) are the molar ratios among DPPC-*d62*, POPG and PA.

DPPC-*d62*–tripalmitin mixed monolayer

The DPPC-*d62*–tripalmitin mixed monolayer was investigated to better understand film metastability. A DPPC monolayer under dynamic compression is in a nonequilibrium state and can have unique properties distinct from the monolayer in the equilibrium state (3,59). For example, a DPPC monolayer can reach near-zero surface tension (corresponding to 72 mN/m surface pressure) under dynamic compression, but it can only attain about 45 mN/m surface pressure under its equilibrium spreading condition. *In vivo*, lung surfactant monolayers can also sustain high surface pressure for an extended period of time without collapsing in static lungs. This suggests that lung surfactant maintains a metastable state during breathing. Finding factors that affect the nonequilibrium state and metastability of lung surfactant is an important issue in understanding lung surfactant function. Recently captive bubble studies showed that fast compression can be a way to improve the film metastability of lung surfactant (18,19,59). In this section, we reveal that film metastability can be enhanced through the intermolecular interaction using tripalmitin in the mixed monolayer with DPPC.

Two monolayers, a DPPC-*d62* monolayer and a DPPC-*d62*–tripalmitin mixed monolayer, were compressed to a surface pressure of 42 mN/m under the exact same experimental conditions. Once the surface pressure of 42 mN/m was reached, the barriers were halted and the films were allowed to relax. The film relaxation process was monitored in two ways simultaneously: (1) the surface pressure was monitored as a function of time; and (2) BBSFG spectra of the film were obtained in real time. Figure 11 shows the surface pressure and time relationship of the DPPC-*d62* monolayer and the DPPC-*d62*–triplamitin (1:1) mixed monolayer during a 30 min period. The two monolayers showed distinctly different film relaxation behavior. The DPPC-*d62* monolayer experienced a continuous surface pressure drop after the barriers were halted during the 30 min monitoring period, suggesting film instability. In contrast, the DPPC-*d62*–tripalmitin monolayer revealed a slight pressure increase right after the barrier halting

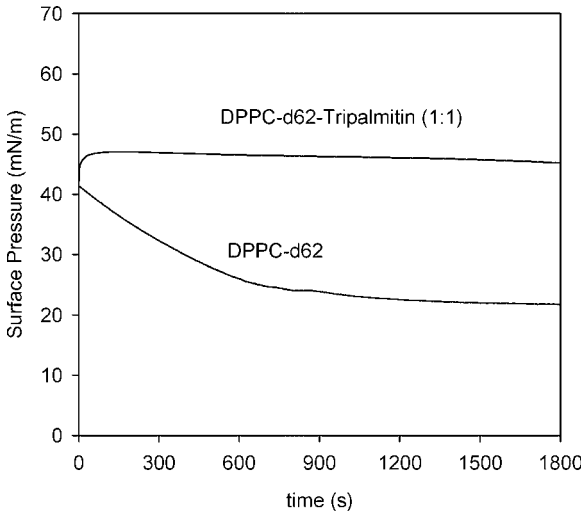

Figure 11. Film relaxation curves of DPPC-*d62* monolayer and DPPC–tripalmitin mixed monolayer on a pure water subphase at 24°C.

and then the surface pressure remained nearly unchanged during the 30 min monitoring period, suggesting enhanced film stability.

Figure 12A,B shows the selected BBSFG spectral snapshots taken during the film relaxation process of the two monolayers. For the DPPC-*d62* monolayer, as indicated by arrows, during the film relaxation both the CD_2-SS and the CD_2-AS appear, revealing gauche defects in the DPPC-*d62* tails. This indicates DPPC-*d62* loss during film relaxation. The DPPC-*d62* in the compacted LC phase is unable to sustain itself and relaxes. During the relaxation period, the DPPC film begins to show spectral features of DPPC in the LE phase because of decreased surface number density of DPPC-*d62*.

For the DPPC-*d62*–tripalmitin monolayer, the scenario is very different. The five spectra in Fig. 12B are nearly identical to each other, indicating that DPPC-*d62* is in a metastable state and retains its organization within the mixed film with little to no relaxation. The improved film metastability of DPPC-*d62* because of the presence of tripalmitin is attributed to the existence of intermolecular interactions between DPPC-*d62* and tripalmitin. To gain insight into this intermolecular interaction, BBSFG was employed to investigate spectral frequency shifts. Figure 13 shows the BBSFG spectra of DPPC-*d62* and DPPC-*d62*–tripalmitin at 42 mN/m. Comparison reveals an obvious frequency redshift of the CD_3-FR peak in the DPPC-*d62*–tripalmitin mixture with respect to that of DPPC-*d62*. Fitting results show that the CD_3-FR shifted from 2122 cm^{-1} for the DPPC-*d62* film to 2119 cm^{-1} for the DPPC-*d62*–tripalmitin film. The observed frequency shift of 3 cm^{-1} suggests a chain-chain interaction between DPPC-*d62* and tripalmitin. This small shift is indicative of a slightly stronger intermolecular interaction between DPPC and tripalmitin chains relative to DPPC–DPPC chain interactions. This intermolecular interaction between DPPC and tripalmitin provides a substantial contribution to the enhanced film stability of the DPPC.

DPPC-*d62*–POPG–PA–KL_4 mixed monolayer

Proper lung surfactant function requires good film respreading properties. Respreading is a process by which surfactant molecules that are ejected into interfacial aggregates of the collapse phases during compression are able to reenter and spread back into the film during expansion (3). Good respreading properties can minimize interfacial surfactant loss, which is crucial in reducing lung surfactant depletion during the breathing cycle. The respreading of a lung surfactant monolayer is believed to depend on surfactant molecular structures and intermolecular interactions, especially interactions between lipids and surfactant proteins such as SP-B and SP-C (7–9,12–14,24,27–29,37,38). There is a paucity of methodologies that can measure interfacial surfactant loss in a molecularly-specific way. Using BBSFG to monitor the respreading process in real time, the interfacial loss of DPPC is quantitatively measured in a complex lung surfactant mixture of DPPC-*d62*–POPG–PA–KL_4 (103). This recent investigation (103) is summarized here.

Figure 14 shows the compression and expansion isotherms of a complex surfactant monolayer containing DPPC-*d62*, POPG, PA and KL_4. Under our experimental setup and conditions, it takes 876 s to complete a compression isotherm and another 876 s to complete an expansion isotherm. The compression and expansion processes were monitored in real time with BBSFG spectroscopy. Because the BBSFG acquisition time is not infinitely small, each

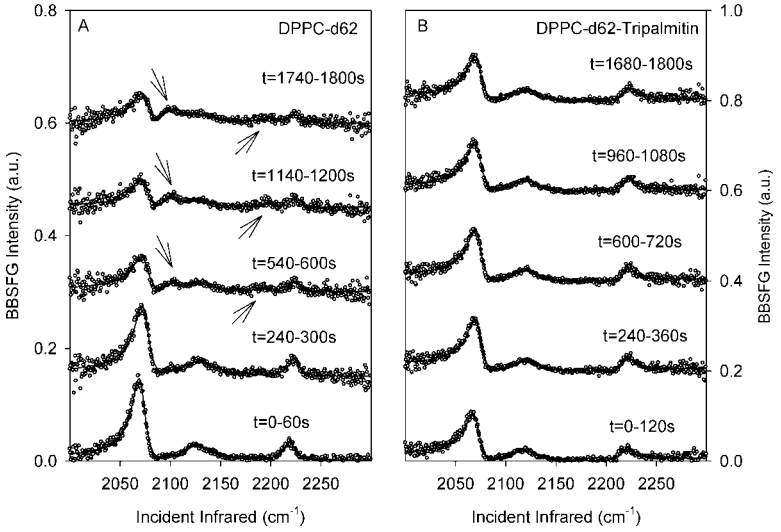

Figure 12. A: Selected BBSFG spectra during the 30 min film relaxation of DPPC-*d62* monolayer with a 1 min spectral acquisition time. B: Selected BBSFG spectra during the 30 min film relaxation of DPPC-*d62*–tripalmitin mixed monolayer with a 2 min spectral acquisition time.

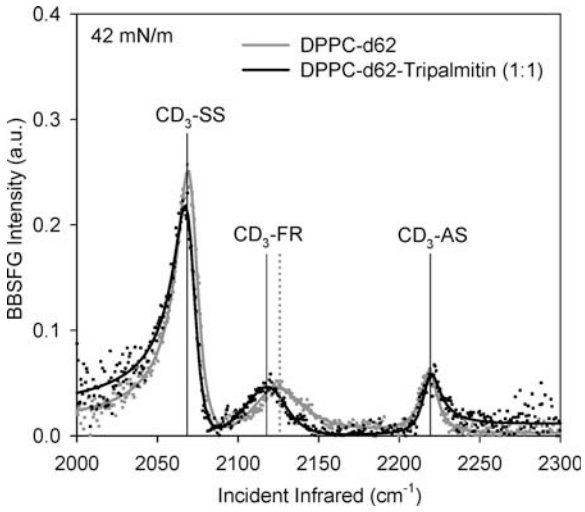

Figure 13. BBSFG spectra of DPPC-*d62* monolayer and DPPC-*d62*–tripalmitin mixed monolayer in the C-D stretching region with spectral assignments at 42 mN/m on a pure water subphase at 24°C. Solid lines are spectral fits; (1:1) is the molar ratio between DPPC-*d62* and tripalmitin.

spectrum will cover a segment of the isotherm. The isotherm is divided into 30 segments and each segment is spectroscopically covered by a BBSFG spectrum with a 29.2 s acquisition time. In our study, each segment is referred to as a time window. Because under the same time windows, lipid molecules occupy the same trough areas during compression and expansion, the number density variation of the lipid will be directly related to the percentage of the interfacial loss of the lipid. The real-time acquired BBSFG spectra of DPPC-*d62* were used to gain information about the surface number density variation of DPPC-*d62* during the respreading of the DPPC-*d62*–POPG–PA–KL_4 monolayer. In particular, the intensity of the CD_3-SS band of DPPC-*d62* was used as a measure of the number density variation of DPPC-*d62* before and after respreading.

Figure 15 shows the BBSFG spectra of DPPC-*d62* during compression and expansion for time window 28. The decreased DPPC-*d62* BBSFG intensity after respreading suggests interfacial

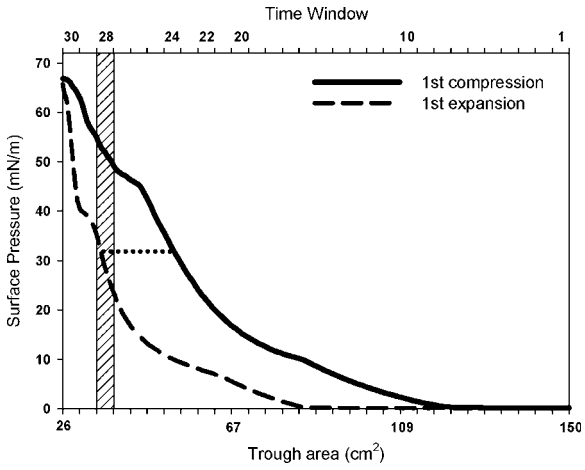

Figure 14. Compression and expansion isotherms of the DPPC-*d62*–POPG–PA–KL_4 (formula: 66/22/7/5 by weight) on a buffer subphase (pH = 7) at 24°C. Vertical column is a representative time window; horizontal dotted line indicates the trough area reduction.

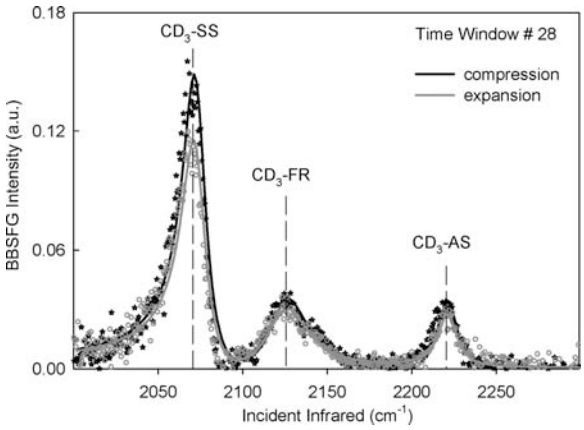

Figure 15. BBSFG spectra of DPPC-*d62* in DPPC-*d62*–POPG–PA–KL_4 monolayer in time window 28. Black spectrum is the BBSFG spectrum for the first compression isotherm segment; gray spectrum is the BBSFG spectrum for the first expansion isotherm segment; solid lines are spectral fits.

loss of DPPC-*d62*. To quantify the DPPC-*d62* loss on the basis of the peak intensity change of CD_3-SS, the orientation effect must be carefully considered. As shown in equation (4), the square root of the SFG intensity of the CD_3-SS peak is related to the number density (N), but complicated by the orientation distribution (73).

$$\sqrt{I_{ssp}(CD_3 - SS)} \propto \chi_{yyz} = \frac{1}{2} N\beta_{ccc}[\langle \cos\theta \rangle (1+R) - \langle \cos^3\theta \rangle (1-R)] \qquad (4)$$

In equation (4), R and β_{ccc} are constants for a given molecule; θ is the orientation angle of the C_3 symmetry axis of the methyl group with respect to the surface normal; and $\langle\ \rangle$ represents the orientation average because the orientation angle has a distribution function. In Fig. 15, both of the two spectra carry the spectral feature of DPPC-*d62* in the LC phase (refer to the DPPC-*d62* spectrum at 42 mN/m in Fig. 4). For the LC phase, it is reasonable to assume a δ function for the orientation angle distribution for the methyl groups in the DPPC tails. Therefore, both $\langle\cos\theta\rangle$ and $\langle\cos^3\theta\rangle$ can be simplified to be $\cos\theta$ and $\cos^3\theta$. Furthermore, fitting results showed that the relative intensity ratio between the CD_3-AS and CD_3-SS peaks for the two spectra in Fig. 15 were nearly the same, demonstrating that the orientation angles of the two cases were the same. Now equation (4) can be simply expressed in the form of equation (5). According to equation (5), the intensity variation of the CD_3-SS peaks for the compression and expansion of time window 28 can be easily used to measure the number density variation of DPPC-*d62*.

$$\sqrt{I_{ssp}(CD_3 - SS)} \propto N \qquad (5)$$

Based on equation (5), by comparing the fitted peak intensity of the CD_3-SS peak of the two spectra in Fig. 15, a 12% interfacial loss of DPPC-*d62* after respreading is revealed. Equation (5) also sets a standard for choosing the suitable time windows. Not all of the 30 time windows follow the relationship in equation (5). For example, for those time windows covering low surface pressures, DPPC-*d62* will be in the LE phase and the orientation angle distribution will not be a simple δ function, and the relationship between the SFG intensity and N will not follow the simple relationship described in equation (5).

The interesting phenomenon revealed by Figs. 14 and 15 is that the isotherm measurements show a 34% trough area reduction for the expansion curve as compared with the compression curve, whereas the BBSFG measurement shows only a 12% DPPC-*d62* loss during respreading. This suggests that the interfacial losses of the four components are not uniform. If the four monolayer components had a uniform interfacial loss during respreading, the expansion isotherm would be simply shifted to the left by a trough area reduction of 12%. The 34% trough area reduction is because of a disproportionately high loss of non-DPPC components. Therefore, results from Fig. 14 and Fig. 15 reveal a DPPC enrichment during monolayer respreading.

CONCLUSIONS

In this review, recent results on the molecular level details of lung surfactant monolayers using vibrational sum frequency generation spectroscopy coupled to a Langmuir film balance were presented. In summary, model monolayers constituted with DPPC-*d62*, PA, POPG, tripalmitin and KL_4 were explored. VSFG, using BBSFG technology, provided direct evidence for the condensing effect of PA on DPPC and the fluidizing effect of POPG on DPPC. The balance between these two effects was further investigated in the DPPC-*d62*–POPG–PA mixed monolayers. Film relaxation behavior of DPPC under the influence of tripalmitin was also investigated, and it was determined that tripalmitin enhanced the DPPC film metastability. A DPPC-enrichment process was revealed from the real-time spectroscopic probing of the respreading of the complex lung surfactant mixture containing DPPC-*d62*, POPG, PA and KL_4. These investigations showed the significance of monolayer composition on the monolayer interfacial structures and demonstrated the potential of VSFG as a powerful surface technique to elucidate the composition–function relationship of lung surfactant.

FUTURE PERSPECTIVES

In the past several decades, many breakthroughs in lung surfactant research have been revealed. New concepts and models proposed based on recent results using a variety of experimental and theoretical tools have improved our understanding about how lung surfactant functions. Recently, investigators have been combining traditionally macroscopic (thermodynamic) measurements with microscopic and selective spectroscopic tools to further deconvolve the inferred mechanisms of functional and dysfunctional lung surfactant. In the realm of spectroscopy, nonlinear optical tools are now being applied as shown in this review, in addition to reflection absorption infrared spectroscopic studies as briefly discussed here, to further investigate lung surfactant biophysics. Additional tools such as coherent anti-Stokes Raman scattering microscopy and VSFG microscopy would further improve the state of understanding. Vibrational spectroscopies offer insight into the intramolecular and intermolecular interactions and provide an understanding as to why one will observe specific phenomena (*e.g.* domain formation and isotherm behavior) from more traditional microscopy and thermodynamic experiments. This molecular perspective from surface selective spectroscopies with different selection rules provides critically important interaction and conformational information that then allows for better design of lung surfactant replacement formulations. It is clear that there is no one experimental tool that will solve all of the unknowns with respect to lung function and dysfunction; however, it is also clear that with the use of more sensitive and complementary techniques, and with studying more complex model systems and natural lung surfactant systems, new insights can and will emerge. Lung dysfunction has many underlying causes, and by precisely and accurately understanding lung surfactant component interactions, using an array of old and new techniques, researchers can make a significant impact.

SUPPLEMENTAL MATERIALS

Figures S1–S5 (additional isotherms) can be found at DOI: 10.1562/2006-06-30-IR-958.s1.

Acknowledgements—The authors acknowledge the Arnold and Mabel Beckman Foundation for funding this research through a Beckman Young Investigator Award.

REFERENCES

1. Goerke, J. and J. A. Clements (1986) Alveolar surface tension and lung surfactant. In *Handbook of Physiology: The Respiratory System,* Vol. III (Edited by P. T. Mackelm and J. Mead), pp. 247–261. American Physiology Society, Washington.
2. Goerke, J. (1998) Pulmonary surfactant: Functions and molecular composition. *Biochim. Biophys. Acta* **1408**, 79–89.
3. Notter, R. H. (2000) *Lung Surfactants: Basic Science and Clinical Applications.* Marcel Dekker, New York.
4. Creuwels, L. A. J. M., L. M. G. Van Golde and H. P. Haagsman (1997) The pulmonary surfactant system: Biochemical and clinical aspects. *Lung* **175**, 1–39.
5. Veldhuizen, R., K. Nag, S. Orgeig and F. Possmayer (1998) The role of lipids in pulmonary surfactant. *Biochim. Biophys. Acta* **1408**, 90–108.
6. McIntyre, R. C., Jr., E. J. Pulido, D. D. Bensard, B. D. Shames and E. Abraham (2000) Thirty years of clinical trials in acute respiratory distress syndrome. *Crit. Care Med.* **28**, 3314–3331.
7. Notter, R. H., S. A. Tabak and R. D. Mavis (1980) Surface properties of binary mixtures of some pulmonary surfactant components. *J. Lipid Res.* **21**, 10–22.
8. Fleming, B. D. and K. M. W. Keough (1988) Surface respreading after collapse of monolayers containing major lipids of pulmonary surfactant. *Chem. Phys. Lipids* **49**, 81–86.
9. Wang, Z., S. B. Hall and R. H. Notter (1995) Dynamic surface activity of films of lung surfactant phospholipids, hydrophobic proteins, and neutral lipids. *J. Lipid Res.* **36**, 1283–1293.
10. Ma, J., S. Koppenol, H. Yu and G. Zografi (1998) Effects of a cationic and hydrophobic peptide, KL4, on model lung surfactant lipid monolayers. *Biophys. J.* **74**, 1899–1907.
11. Longo, M. L., A. M. Bisagno, J. A. Zasadzinski, R. Bruni and A. J. Waring (1993) A function of lung surfactant protein SP-B. *Science* **261**, 453–456.
12. Liu, H., R. Z. Lu, J. G. Turcotte and R. H. Notter (1994) Dynamic interfacial properties of surface-excess films of phospholipids and phosphonolipid analogs. I. Effects of pH. *J. Colloid Interface Sci.* **167**, 378–390.
13. Liu, H., J. G. Turcotte and R. H. Notter (1994) Dynamic interfacial properties of surface-excess films of phospholipids and phosphonolipid analogs. II. Effects of chain linkage and headgroup structure. *J. Colloid Interface Sci.* **167**, 391–400.
14. Taneva, S. G. and K. M. W. Keough (1994) Dynamic surface properties of pulmonary surfactant proteins SP-B and SP-C and their mixtures with dipalmitoylphosphatidylcholine. *Biochemistry* **33**, 14660–14670.
15. Chang, C.-H., K. A. Coltharp, S. Y. Park and E. I. Franses (1996) Surface tension measurements with the pulsating bubble method. *Colloids Surf., A* **114**, 185–197.
16. Schurch, S., F. H. Green and H. Bachofen (1998) Formation and structure of surface films: Captive bubble surfactometry. *Biochim. Biophys. Acta* **1408**, 180–202.
17. Crane, J. M., G. Putz and S. B. Hall (1999) Persistence of phase coexistence in disaturated phosphatidylcholine monolayers at high surface pressures. *Biophys. J.* **77**, 3134–3143.

18. Crane, J. M. and S. B. Hall (2001) Rapid compression transforms interfacial monolayers of pulmonary surfactant. *Biophys. J.* **80**, 1863–1872.
19. Smith, E. C., J. M. Crane, T. G. Laderas and S. B. Hall (2003) Metastability of a supercompressed fluid monolayer. *Biophys. J.* **85**, 3048–3057.
20. Zuo, Y. Y., R. Gitiafroz, E. Acosta, Z. Policova, P. N. Cox, M. L. Hair and A. W. Neumann (2005) Effect of humidity on the adsorption kinetics of lung surfactant at air-water interfaces. *Langmuir* **21**, 10593–10601.
21. Lipp, M. M., K. Y. Lee, J. A. Zasadzinski and A. J. Waring (1996) Phase and morphology changes in lipid monolayers induced by SP-B protein and its amino-terminal peptide. *Science* **273**, 1196–1199.
22. Nag, K., J. Perez-Gil, A. Cruz and K. M. W. Keough (1996) Fluorescently labeled pulmonary surfactant protein C in spread phospholipid monolayers. *Biophys. J.* **71**, 246–256.
23. Lipp, M. M., K. Y. C. Lee, A. Waring and J. A. Zasadzinski (1997) Fluorescence, polarized fluorescence, and Brewster angle microscopy of palmitic acid and lung surfactant protein B monolayers. *Biophys. J.* **72**, 2783–2804.
24. Lipp, M. M., K. Y. C. Lee, D. Y. Takamoto, J. A. Zasadzinski and A. J. Waring (1998) Coexistence of buckled and flat monolayers. *Phys. Rev. Lett.* **81**, 1650–1653.
25. Nag, K., J. Perez-Gil, M. L. Ruano, L. A. Worthman, J. Stewart, C. Casals and K. M. Keough (1998) Phase transitions in films of lung surfactant at the air-water interface. *Biophys. J.* **74**, 2983–2995.
26. Kruger, P., M. Schalke, Z. Wang, R. H. Notter, R. A. Dluhy and M. Losche (1999) Effect of hydrophobic surfactant peptides SP-B and SP-C on binary phospholipid monolayers. I. Fluorescence and dark-field microscopy. *Biophys. J.* **77**, 903–914.
27. Krol, S., M. Ross, M. Sieber, S. Kunneke, H.-J. Galla and A. Janshoff (2000) Formation of three-dimensional protein-lipid aggregates in monolayer films induced by surfactant protein B. *Biophys. J.* **79**, 904–918.
28. Takamoto, D. Y., M. M. Lipp, A. von Nahmen, K. Y. C. Lee, A. J. Waring and J. A. Zasadzinski (2001) Interaction of lung surfactant proteins with anionic phospholipids. *Biophys. J.* **81**, 153–169.
29. Ding, J., D. Y. Takamoto, A. von Nahmen, M. M. Lipp, K. Y. C. Lee, A. J. Waring and J. A. Zasadzinski (2001) Effects of lung surfactant proteins, SP-B and SP-C, and palmitic acid on monolayer stability. *Biophys. J.* **80**, 2262–2272.
30. Bringezu, F., J. Ding, G. Brezesinski and J. A. Zasadzinski (2001) Changes in model lung surfactant monolayers induced by palmitic acid. *Langmuir* **17**, 4641–4648.
31. Piknova, B., W. R. Schief, V. Vogel, B. M. Discher and S. B. Hall (2001) Discrepancy between phase behavior of lung surfactant phospholipids and the classical model of surfactant function. *Biophys. J.* **81**, 2172–2180.
32. Kruger, P., J. E. Baatz, R. A. Dluhy and M. Losche (2002) Effect of hydrophobic surfactant protein SP-C on binary phospholipid monolayers. Molecular machinery at the air/water interface. *Biophys. Chem.* **99**, 209–228.
33. Discher, B. M., K. M. Maloney, W. R. Schief, D. W. Grainger, V. Vogel and S. B. Hall (1996) Lateral phase separation in interfacial films of pulmonary surfactant. *Biophys. J.* **71**, 2583–2590.
34. Discher, B. M., W. R. Schief, V. Vogel and S. B. Hall (1999) Phase separation in monolayers of pulmonary surfactant phospholipids at the air-water interface: Composition and structure. *Biophys. J.* **77**, 2051–2061.
35. Schief, W. R., M. Antia, B. M. Discher, S. B. Hall and V. Vogel (2003) Liquid-crystalline collapse of pulmonary surfactant monolayers. *Biophys. J.* **84**, 3792–3806.
36. Alonso, C., T. Alig, J. Yoon, F. Bringezu, H. Warriner and J. A. Zasadzinski (2004) More than a monolayer: Relating lung surfactant structure and mechanics to composition. *Biophys. J.* **87**, 4188–4202.
37. Ding, J., I. Doudevski, H. E. Warriner, T. Alig, J. A. Zasadzinski, A. J. Waring and M. A. Sherman (2003) Nanostructure changes in lung surfactant monolayers induced by interactions between palmitoyloleoylphosphatidylglycerol and surfactant protein B. *Langmuir* **19**, 1539–1550.
38. von Nahmen, A., M. Schenk, M. Sieber and M. Amrein (1997) The structure of a model pulmonary surfactant as revealed by scanning force microscopy. *Biophys. J.* **72**, 463–469.
39. Flanders, B. N., S. A. Vickery and R. C. Dunn (2001) Imaging of monolayers composed of palmitic acid and lung surfactant protein B. *J. Microsc.* **202**, 379–385.
40. Lee, K. Y. C., J. Majewski, T. L. Kuhl, P. B. Howes, K. Kjaer, M. M. Lipp, A. J. Waring, J. A. Zasadzinski and G. S. Smith (2001) Synchrotron X-ray study of lung surfactant-specific protein SP-B in lipid monolayers. *Biophys. J.* **81**, 572–585.
41. Lee, K. Y. C., A. Gopal, A. von Nahmen, J. A. Zasadzinski, J. Majewski, G. S. Smith, P. B. Howes and K. Kjaer (2002) Influence of palmitic acid and hexadecanol on the phase transition temperature and molecular packing of dipalmitoylphosphatidyl-choline monolayers at the air-water interface. *J. Chem. Phys.* **116**, 774–783.
42. Dluhy, R. A., K. E. Reilly, R. D. Hunt, M. L. Mitchell, A. J. Mautone and R. Mendelsohn (1989) Infrared spectroscopic investigations of pulmonary surfactant. Surface film transitions at the air-water interface and bulk phase thermotropism. *Biophys. J.* **56**, 1173–1181.
43. Pastrana-Rios, B., C. R. Flach, J. W. Brauner, A. J. Mautone and R. Mendelsohn (1994) A direct test of the ''squeeze-out'' hypothesis of lung surfactant function. External reflection FT-IR at the air/water interface. *Biochemistry* **33**, 5121–5127.
44. Mendelsohn, R., J. W. Brauner and A. Gericke (1995) External infrared reflection absorption spectrometry of monolayer films at the air-water interface. *Annu. Rev. Phys. Chem.* **46**, 305–334.
45. Cai, P., C. R. Flach and R. Mendelsohn (2003) An infrared reflection-absorption spectroscopy study of the secondary structure in (KL4)4K, a therapeutic agent for respiratory distress syndrome, in aqueous monolayers with phospholipids. *Biochemistry* **42**, 9446–9452.
46. Brockman, J. M., Z. Wang, R. H. Notter and R. A. Dluhy (2003) Effect of hydrophobic surfactant proteins SP-B and SP-C on binary phospholipid monolayers II. Infrared external reflectance-absorption spectroscopy. *Biophys. J.* **84**, 326–340.
47. Flach, C. R., P. Cai, D. Dieudonne, J. W. Brauner, K. M. W. Keough, J. Stewart and R. Mendelsohn (2003) Location of structural transitions in an isotopically labeled lung surfactant SP-B peptide by IRRAS. *Biophys. J.* **85**, 340–349.
48. Shanmukh, S., N. Biswas, A. J. Waring, F. J. Walther, Z. Wang, Y. Chang, R. H. Notter and R. A. Dluhy (2005) Structure and properties of phospholipid-peptide monolayers containing monomeric SP-B(1-25) II. Peptide conformation by infrared spectroscopy. *Biophys. Chem.* **113**, 233–244.
49. Wang, L., P. Cai, H.-J. Galla, H. He, C. R. Flach and R. Mendelsohn (2005) Monolayer-multilayer transitions in a lung surfactant model: IR reflection-absorption spectroscopy and atomic force microscopy. *Eur. Biophys. J.* **34**, 243–254.
50. Galla, H. J., N. Bourdos, A. von Nahmen, M. Amrein and M. Sieber (1998) The role of pulmonary surfactant protein C during the breathing cycle. *Thin Solid Films* **327–329**, 632–635.
51. Bourdos, N., F. Kollmer, A. Benninghoven, M. Ross, M. Sieber and H.-J. Galla (2000) Analysis of lung surfactant model systems with time-of-flight secondary ion mass spectrometry. *Biophys. J.* **79**, 357–369.
52. Harbottle, R. R., K. Nag, N. S. McIntyre, F. Possmayer and N. O. Petersen (2003) Molecular organization revealed by time-of-flight secondary ion mass spectrometry of a clinically used extracted pulmonary surfactant. *Langmuir* **19**, 3698–3704.
53. Chung, J. B., R. E. Hannemann and E. I. Franses (1990) Surface analysis of lipid layers at air/water interfaces. *Langmuir* **6**, 1647–1655.
54. Williams, A. D., J. M. Wilkin and R. A. Dluhy (1997) The phase behavior of binary lipid monolayers as determined by surface chemistry and IR spectroscopy. *Mikrochim. Acta Suppl.* **14**, 687–689.
55. Lee, H., S. K. Kandasamy and R. G. Larson (2005) Molecular dynamics simulations of the anchoring and tilting of the lung-surfactant peptide SP-B1-25 in palmitic acid monolayers. *Biophys. J.* **89**, 3807–3821.
56. Kandasamy, S. K. and R. G. Larson (2005) Molecular dynamics study of the lung surfactant peptide SP-B1-25 with DPPC monolayers: Insights into interactions and peptide position and orientation. *Biophys. J.* **88**, 1577–1592.
57. Freites, J. A., Y. Choi and D. J. Tobias (2003) Molecular dynamics simulations of a pulmonary surfactant protein B peptide in a lipid monolayer. *Biophys. J.* **84**, 2169–2180.
58. Keough, K. M. W. (1992) Physical chemistry of pulmonary surfactant in the terminal air spaces. In *Pulmonary Surfactant from Molecular*

Biology to Clinical Practice. (Edited by B. Robertson, L. M. G. Van Golde and J. J. Batenburg), pp. 109–164. Elsevier, Amsterdam.
59. Rugonyi, S. and S. B. Hall (2005) The basis of low surface tensions in the lungs. In *Lung Surfactant Function and Disorder*. (Edited by K. Nag), pp. 173–189. Taylor & Francis Group, Boca Raton, FL.
60. Zasadzinski, J. A., J. Ding, H. E. Warriner, F. Bringezu and A. J. Waring (2001) The physics and physiology of lung surfactants. *Curr. Opin. Colloid Interface Sci.* **6**, 506–513.
61. Tanaka, Y., T. Takei, T. Aiba, K. Masuda, A. Kiuchi and T. Fujiwara (1986) Development of synthetic lung surfactants. *J. Lipid Res.* **27**, 475–485.
62. Pfister, R. H. and R. F. Soll (2005) New synthetic surfactants: The next generation? *Biol. Neonate* **87**, 338–344.
63. Cochrane, C. G. and S. D. Revak (1991) Pulmonary surfactant protein B (SP-B): Structure-function relationships. *Science* **254**, 566–568.
64. Ishibashi, T.-A. and H. Onishi (2002) Multiplex infrared-visible sum-frequency spectrometer with a phase-conjugated pulse mixing device for narrow-bandwidth visible probe generation. *Appl. Spectrosc.* **56**, 1298–1302.
65. Zhu, X. D., H. Suhr and Y. R. Shen (1987) Surface vibrational spectroscopy by infrared-visible sum frequency generation. *Phys. Rev. B* **35**, 3047–3050.
66. Hunt, J. H., P. Guyot-Sionnest and Y. R. Shen (1987) Observation of C-H stretch vibrations of monolayers of molecules using optical sum-frequency generation. *Chem. Phys. Lett.* **133**, 189–192.
67. Guyot-Sionnest, P., J. H. Hunt and Y. R. Shen (1987) Sum-frequency vibrational spectroscopy of a Langmuir film: Study of molecular orientation of a two-dimensional system. *Phys. Rev. Lett.* **59**, 1597–1600.
68. Bain, C. D. (1995) Sum-frequency vibrational spectroscopy of the solid/liquid interface. *J. Chem. Soc. Faraday Trans.* **91**, 1281–1296.
69. Conboy, J. C., M. C. Messmer and G. L. Richmond (1996) Investigation of surfactant conformation and order at the liquid-liquid interface by total internal reflection sum-frequency vibrational spectroscopy. *J. Phys. Chem.* **100**, 7617–7622.
70. Walker, R. A., J. C. Conboy and G. L. Richmond (1997) Molecular structure and ordering of phospholipids at a liquid-liquid interface. *Langmuir* **13**, 3070–3073.
71. Walker, R. A., J. A. Gruetzmacher and G. L. Richmond (1998) Phosphatidylcholine monolayer structure at a liquid-liquid interface. *J. Am. Chem. Soc.* **120**, 6991–7003.
72. Richter, L. J., T. P. Petralli-Mallow and J. C. Stephenson (1998) Vibrationally resolved sum-frequency generation with broad-bandwidth infrared pulses. *Opt. Lett.* **23**, 1594–1596.
73. Zhuang, X., P. B. Miranda, D. Kim and Y. R. Shen (1999) Mapping molecular orientation and conformation at interfaces by surface nonlinear optics. *Phys. Rev. B* **59**, 12632–12640.
74. Miranda, P. B. and Y. R. Shen (1999) Liquid interfaces: A study by sum-frequency vibrational spectroscopy. *J. Phys. Chem. B* **103**, 3292–3307.
75. Richmond, G. L. (2002) Molecular bonding and interactions at aqueous surfaces as probed by vibrational sum frequency spectroscopy. *Chem. Rev.* **102**, 2693–2724.
76. Chen, Z., Y. R. Shen and G. A. Somorjai (2002) Studies of polymer surfaces by sum frequency generation vibrational spectroscopy. *Annu. Rev. Phys. Chem.* **53**, 437–465.
77. Kim, G., M. C. Gurau, S.-M. Lim and P. S. Cremer (2003) Investigations of the orientation of a membrane peptide by sum frequency spectroscopy. *J. Phys. Chem. B* **107**, 1403–1409.
78. Al-Abadleh, H. A., A. B. Voges, P. A. Bertin, S. T. Nguyen and F. M. Geiger (2004) Chromium(VI) binding to functionalized silica/water interfaces studied by nonlinear optical spectroscopy. *J. Am. Chem. Soc.* **126**, 11126–11127.
79. Rangwalla, H. and A. Dhinojwala (2004) Probing hidden polymeric interfaces using IR-visible sum-frequency generation spectroscopy. *J. Adhesion* **80**, 37–59.
80. Liu, J. and J. C. Conboy (2004) Phase transition of a single lipid bilayer measured by sum-frequency vibrational spectroscopy. *J. Am. Chem. Soc.* **126**, 8894–8895.
81. Bonn, M., S. Roke, O. Berg, L. B. F. Juurlink, A. Stamouli and M. Mueller (2004) A molecular view of cholesterol-induced condensation in a lipid monolayer. *J. Phys. Chem. B* **108**, 19083–19085.
82. Holman, J., P. B. Davies, T. Nishida, S. Ye and D. J. Neivandt (2005) Sum frequency generation from Langmuir-Blodgett multilayer films on metal and dielectric substrates. *J. Phys. Chem. B* **109**, 18723–18732.
83. Wang, J., M. L. Clarke, X. Chen, M. A. Even, W. C. Johnson and Z. Chen (2005) Molecular studies on protein conformations at polymer/liquid interfaces using sum frequency generation vibrational spectroscopy. *Surf. Sci.* **587**, 1–11.
84. Gopalakrishnan, S., D. Liu, H. C. Allen, M. Kuo and M. J. Shultz (2006) Vibrational spectroscopic studies of aqueous interfaces: Salts, acids, bases, and nanodrops. *Chem. Rev.* **106**, 1155–1175.
85. Hirose, C., N. Akamatsu and K. Domen (1992) Formulas for the analysis of the surface SFG spectrum and transformation coefficients of cartesian SFG tensor components. *Appl. Spectrosc.* **46**, 1051–1072.
86. Moad, A. J. and G. J. Simpson (2004) A unified treatment of selection rules and symmetry relations for sum-frequency and second harmonic spectroscopies. *J. Phys. Chem. B* **108**, 3548–3562.
87. Ma, G. and H. C. Allen (2006) DPPC Langmuir monolayer at the air-water interface: Probing the tail and head groups by vibrational sum frequency generation spectroscopy. *Langmuir* **22**, 5341–5349.
88. Gaines, G. L. (1966) *Insoluble Monolayers at Liquid-Gas Interfaces*. Interscience Publishers, New York.
89. Kaganer, V. M., H. Mohwald and P. Dutta (1999) Structure and phase transitions in Langmuir monolayers. *Rev. Mod. Phys.* **71**, 779–819.
90. Sunder, S., D. G. Cameron, H. L. Casal, Y. Boulanger and H. H. Mantsch (1981) Infrared and Raman spectra of specifically deuterated 1,2-dipalmitoyl-sn-glycero-3-phosphocholines. *Chem. Phys. Lipids* **28**, 137–147.
91. Devlin, M. T. and I. W. Levin (1990) Acyl chain packing properties of deuterated lipid bilayer dispersions: Vibrational Raman spectral parameters. *J. Raman Spectrosc.* **21**, 441–451.
92. Ries, H. E., Jr. and H. Swift (1987) Twisted double-layer ribbons and the mechanism for monolayer collapse. *Langmuir* **3**, 853–855.
93. Birdi, K. S. and D. T. Vu (1994) Structures of collapsed lipid monolayers investigated as Langmuir-Blodgett films by atomic force microscopy. *Langmuir* **10**, 623–625.
94. Ma, G. and H. C. Allen (2007) Condensing effect of palmitic acid on DPPC in mixed Langmuir monolayers. Langmuir, DOI: 10.1021/la061870i.
95. Scott, H. L. and S. Kalaskar (1989) Lipid chains and cholesterol in model membranes: A Monte Carlo study. *Biochemistry* **28**, 3687–3691.
96. Smondyrev, A. M. and M. L. Berkowitz (1999) Structure of dipalmitoylphosphatidylcholine/cholesterol bilayer at low and high cholesterol concentrations: Molecular dynamics simulation. *Biophys. J.* **77**, 2075–2089.
97. Arrondo, J. L., F. M. Goni and J. M. Macarulla (1984) Infrared spectroscopy of phosphatidylcholines in aqueous suspension. A study of the phosphate group vibrations. *Biochim. Biophys. Acta* **794**, 165–168.
98. Harrand, M. (1984) Polarized Raman spectra of oriented dipalmitoylphosphatidylcholine (DPPC). II. Scattering activities of phosphatidylcholine vibrations. *J. Chem. Phys.* **81**, 1–5.
99. Okamura, E., J. Umemura and T. Takenaka (1990) Orientation studies of hydrated dipalmitoylphosphatidylcholine multibilayers by polarized FTIR-ATR spectroscopy. *Biochim. Biophys. Acta* **1025**, 94–98.
100. Wong, P. T., S. E. Capes and H. H. Mantsch (1989) Hydrogen bonding between anhydrous cholesterol and phosphatidylcholines: An infrared spectroscopic study. *Biochim. Biophys. Acta* **980**, 37–41.
101. Mrazkova, E., P. Hobza, M. Bohl, D. R. Gauger and W. Pohle (2005) Hydration-induced changes of structure and vibrational frequencies of methylphosphocholine studied as a model of biomembrane lipids. *J. Phys. Chem. B* **109**, 15126–15134.
102. Bansil, R., J. Day, M. Meadows, D. Rice and E. Oldfield (1980) Laser Raman spectroscopic study of specifically deuterated phospholipid bilayers. *Biochemistry* **19**, 1938–1943.
103. Ma, G. and H. C. Allen (2006) Real-time investigation of lung surfactant respreading with surface vibrational spectroscopy. Langmuir, DOI: 10.1021/la061476k.